JOURNAL OF MATERIALS SCIENCE 30 (1995) 3256–3264

Kinetics of a non-catalytic gas–solid chemical reaction under SHS-like conditions

ZHIGANG ZHOU, G. C. STANGLE
Institute for Self-Propagating High-Temperature Synthesis, New York State College of Ceramic at Alfred University, Alfred, NY 14802, USA

Nitration of metallic tantalum under self-propagating high-temperature synthesis (SHS) conditions (i.e. rapid heating rates 2000–3000 K s^{-1}, and short heating periods 2–100 s) has been studied. Phase analysis and microstructural characterization have been performed. A two-phase mixture region of solid solution TaN_x and tantalum subnitride, namely Ta_2N, was observed in the nitrided tantalum at temperatures of 1600–2600 K and a partial nitrogen pressure of 0.1–0.8 MPa. It was also found that tantalum subnitride phase formed before the formation of Ta–N solid solution throughout the sample during nitration. A theoretical study was conducted in order to determine the intrinsic reaction kinetics of a typical combustion synthesis reaction. A new model was developed to explain all experimental observations. The computer simulation results are in good agreement with experimental data. The results indicate that at sufficiently large heating rates the product layer does not necessarily act as a diffusion barrier that prevents further uptake of nitrogen. The results are helpful in developing an understanding of the mechanism of powder-based SHS.

1. Introduction

The self-propagating high-temperature synthesis (SHS) process can be used to fabricate a large number of advanced ceramic, intermetallic and composite materials [1]. SHS is, in the most simple sense, the exploitation of an exothermic and usually very rapid chemical reaction to form a useful material. A key feature of the process is that the heat required to drive the chemical reaction is supplied from the reaction itself, and not from an external and, therefore, expensive source. Materials that have been successfully synthesized include carbides, borides, nitrides, oxides, intermetallics and rather complex composites. Important applications include electronic materials, and wear-, corrosion- and heat-resistant materials.

The SHS process is complex and incompletely understood. A thorough, fundamental understanding of SHS will require a mechanistic framework that accounts for the distinguishing features of the process: examples include local melting, liquid redistribution, vapour-phase formation, intrinsic chemical reaction kinetics, internal heat transfer by conduction and radiation, external heat transfer by radiation and convection, diffusion, supersaturation, and nucleation and growth of the product phase. Several of these sub-processes may occur simultaneously, and each sub-process may influence some or all of the others. Further, a change of one process parameter (such as particle size, gas pressure, sample aspect ratio, etc.) may modify the relative contribution of each sub-process to the outcome of the overall process. Self-propagating behaviour may thus cease if such a change leads to conditions that are sufficiently unfavourable to self-propagation.

The most central and perhaps least well understood sub-process that occurs during the SHS process is the particle-scale chemical reaction that occurs between reactants. This central sub-process is, of course, that portion of the description of the process that remains once all transport resistances have been accounted for. The principal difficulty in developing a detailed understanding of the intrinsic reaction kinetics arises from the fact that a reactant particle is typically 1–50 μm in diameter and typically experiences heating rates on the order of 10^3–10^5 K s^{-1}. *In situ* experiments are an experimental impossibility. Alternatively, indirect methods that have been used to study the intrinsic kinetics include either (i) reaction quenching (using moderate cooling rates [2]), or (ii) a *post-mortem* analysis [3]. These approaches have yielded qualitative information concerning possible mechanisms for both of the major classes of SHS reactions: gas–solid and solid–solid reactions. Quantitative reaction kinetic expressions have not been forthcoming.

In this study, the intrinsic reaction kinetics of the reaction between a transition metal (tantalum) and a reactive gas (nitrogen) have been studied. The experiments consisted essentially of a diffusion couple that was subjected to heating rates that are characteristic of SHS reactions. Experiments were conducted so that the effects of nitrogen overpressure, sample temperature, and time could be determined quantitatively. A detailed theoretical model was developed in order to aid in the interpretation of the experimental results. A detailed reaction mechanism was deduced. The importance of these results to the more general class of gas–solid SHS reactions is discussed.

0022–2461

2. Experimental procedure

Tantalum nitridation at elevated pressure was conducted in a reaction chamber made of stainless steel. The chamber was equipped with two sets of electrodes that pass through gas-tight electrical feed-throughs for resistively heating the sample, and for the use of a suitable oxygen getter. Fig. 1 is a schematic representation of the reaction chamber. The chamber was fitted with sapphire windows, through which the sample temperature was measured with an infrared pyrometer, and through which the process was observed and recorded using video equipment. A cold-drawn tantalum wire (ÆSAR, 99.95%) that had a diameter of 500×10^{-6} m was used. High-purity nitrogen gas was used in which the oxygen content was less than 5 p.p.m. The wire was placed between the two electrodes and the chamber was filled with nitrogen gas at pressures, p_{N_2}, in the range 0.1–0.8 MPa. Electrical current, i, of 16, 20 or 24 A (corresponding to current densities of 0.82, 1.0 and 1.2×10^8 A m^{-2}) was passed through the tantalum wire for a fixed time, t_{cur}, in the range between 3 and 500 s. The corresponding temperatures to which the samples were raised were determined to be 1600, 2100 and 2600 K, respectively. A schematic representation of a typical current–temperature–time profile used in this study is shown in Fig. 2. The temperature was calculated to reach its maximum in less than 2 s. The reaction continued until the current was turned off, at which point the temperature quickly dropped at the rate of 800 K s^{-1} in the first second and cooled to the ambient temperature in about 10 s.

Specifically, the experimental procedure employed was as follows: (i) the reaction chamber was evacuated to 500 μm Hg; (ii) nitrogen gas was passed through the reaction chamber at a flow rate of 100 cm^3 s^{-1} for more than 2 h; (iii) the reaction chamber was filled with nitrogen gas until it reached the specified pressure; (iv) current was abruptly introduced to the wire and maintained for the pre-determined time period; (v) the wire was rapidly cooled by abruptly discontinuing the applied current; and (vi) the gas pressure in the reaction chamber was reduced to the ambient.

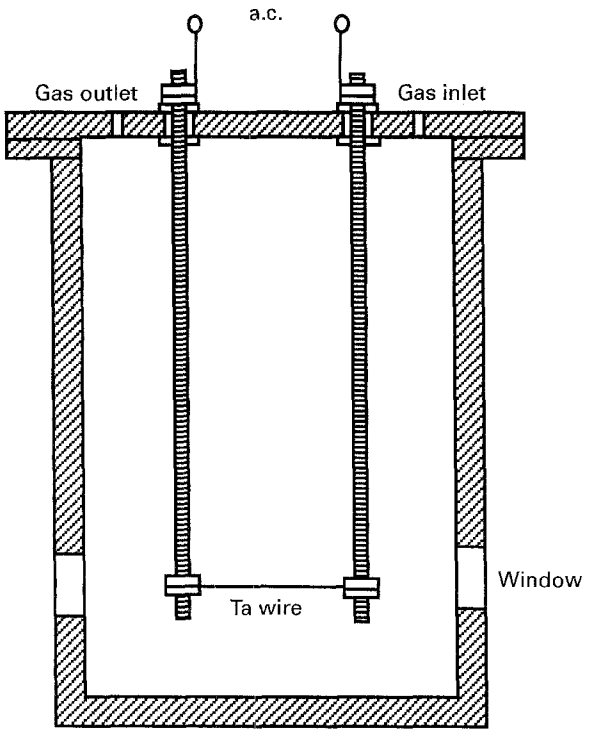

Figure 1 The high-pressure reaction chamber (schematic drawing). A tantalum wire is held between electrodes under a nitrogen atmosphere. When the wire is resistively heated, nitrogen is absorbed. The wire is thus partially nitrided.

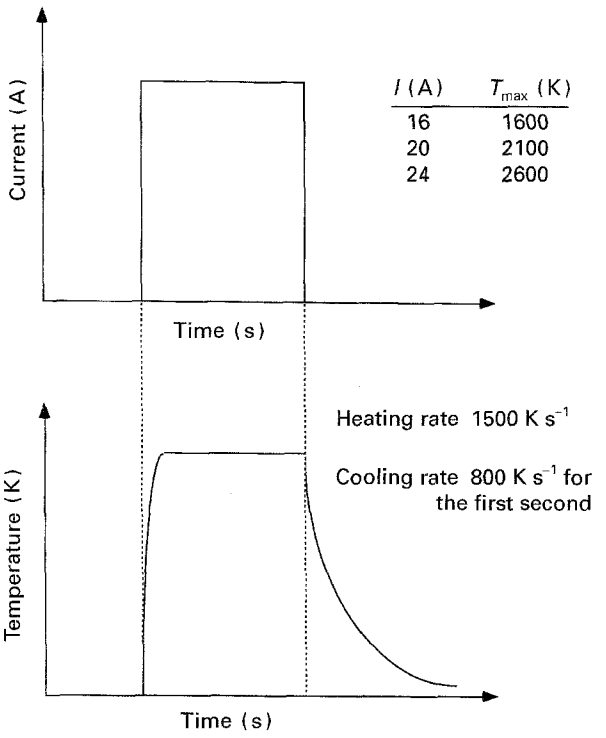

Figure 2 Current and temperature profiles for tantalum wire in gaseous nitrogen at $p_{N_2} = 0.1$ MPa.

Scanning electron microscopy (SEM) was used to observe microstructural changes in the nitrided tantalum wire. The cross-section of the nitrided tantalum wire samples was embedded in an epoxy disc for grinding and polishing. The polished surface of the wire was chemically etched using a mixed acid solution (HNO_3:HF:H_2SO_4) that selectively removed the α-phase and left the β-phase (see also Section 3.1). Quantitative X-ray diffraction (XRD) analysis was used to determine the composition of the nitrided tantalum wire. Both the surface of the nitrided wire and powder obtained by grinding the wire were analysed. The parameters used for the X-ray diffraction analysis were: (i) a scan rate of 1° (2θ) min^{-1}; (ii) a chopper increment of 0.05° (2θ); and (iii) a counting time of 2 s. Finally, the weight of the wire before and after nitridation was measured using a micro-grammatic balance (Fischer Scientific Company) to an accuracy of 0.005 mg.

3. Results and discussion

The primary purpose of this work was to understand the kinetics of tantalum nitridation under SHS conditions. This was accomplished by studying the interaction between a rapidly heated metal wire and a reactive gas. Both thermodynamic and kinetic information

were used to develop a detailed, quantitative understanding of the reaction mechanism. The results of such a study may then be used to form the basis for a quantitative interpretation of the large class of SHS reactions.

3.1. Phase identification and morphology

In order to elucidate the intrinsic mechanism of the Ta–N_2 reaction, a detailed knowledge of the product phases must first be acquired. First, a detailed knowledge of the equilibrium phase diagram is required. Second, the distribution of phases in (i.e. the microstructure of) the partially nitrided wire must be determined. Third, the radial distribution of the volume fraction of each phase must be determined. This information may then ultimately be used to establish a basis upon which a reaction mechanism may be deduced.

In the equilibrium phase diagram for the tantalum–nitrogen system [4], there are various nitride phases such as TaN_x (α phase), Ta_2N_{1-y} (β phase), hexagonal $TaN_{1\pm\varepsilon}$ (ε phase) and cubic $TaN_{1\pm\delta}$ (δ phase) (see also Fig. 3). In the temperature range between 2500 and 3300 K, tantalum and nitrogen form a solid solution, namely TaN_x (for $0 \leq x \leq 0.19$). The various nitrides and solid solutions are stable phases and may co-exist in certain composition and temperature ranges. The nitride phases are typically highly non-stoichiometric in nitrogen. The nitrogen stoichiometry deviation, y, in Ta_2N_{1-y} is in the range of $0 < y < 0.42$ at the temperature of 2600 K. There are, of course, several phases, such as $Ta_4N_{1\pm z}$ (orthorhombic) and Ta_3N_5 (tetragonal) that are known to exist [5, 6], but that have not yet been incorporated into the phase diagram shown in Fig. 3. Therefore, even though the complete tantalum–nitrogen phase diagram can thus be expected to be somewhat more complex, the discussion here will make use of the information contained in Fig. 3.

The distribution of Ta–N phases in the wire following nitridation was as follows. Scanning electron micrographs of the cross-section of the tantalum wire following nitridation are shown in Fig. 4. Fig. 4a–c show the results for reactions that were conducted for time periods of short, intermediate and long duration, respectively. The sample in Fig. 4a was heated in a nitrogen atmosphere ($p_{N_2} = 0.1$ MPa) for 3 s using a current of 20 A ($\approx$ 2100 K). The outermost ring was observed to be thin and not readily seen in the micrograph. Further, because the boundaries between the other rings were seen to be indistinct and not well defined, the corresponding images are shown schematically to the right of the micrographs. The corresponding XRD analysis showed that the outer ring consisted of crystalline Ta_2N_{1-y}, and that the entire (partially nitrided) tantalum wire was a mixture of Ta_2N_{1-y}, TaN_x and tantalum metal. It was determined that the wire actually consisted of a core of metallic tantalum that was enveloped by three concentric layers: a ring of tantalum–nitrogen solid solution (TaN_x, or α phase); a two-phase ring in which both α and β phases were present; and a one-phase ring of β-phase material at the surface. In the two-phase ring, Ta_2N_{1-y} existed in the form of islands dispersed in a continuous matrix of TaN_x solid solution. Fig. 4b shows the result for an intermediate reaction time. The partially nitrided wire was shown to consist of an outer ring, an inner ring, and a central core. XRD analysis showed that the outer ring was Ta_2N_{1-y} (β phase), that the core was TaN_x (α phase) and that the intermediate ring was a two-phase mixture of the α and β phases. In the two-phase ring, β-phase existed in the form of islands embedded in an α-phase matrix. The metallic tantalum core that was present in Fig. 4a was not observed in Fig. 4b. Fig. 4c shows the results for a wire subjected to nitridation for a relatively long period ($t_{cur} = 100$ s). The ring portion was shown by XRD analysis to be the β phase, while the core was a mixture of α and β phases. It is worthwhile to emphasize that in our observation, β phase formed before the formation of α phase throughout the sample. This is different from the observations of Grigoriev *et al.* [7]. They reported that during nitrition of fine wires (100–120 μm diameter) of niobium, titanium and zirconium α phase formed first, and β phase did not form until α phase was saturated with nitrogen up to the solid solution limit. It is of interest to note the existence of mixture of α + β two-phase region beside α single-phase region and β single-phase region. The boundary of (α + β)/β is distinct and sharp while the boundary of α/(α + β) is relatively indistinct.

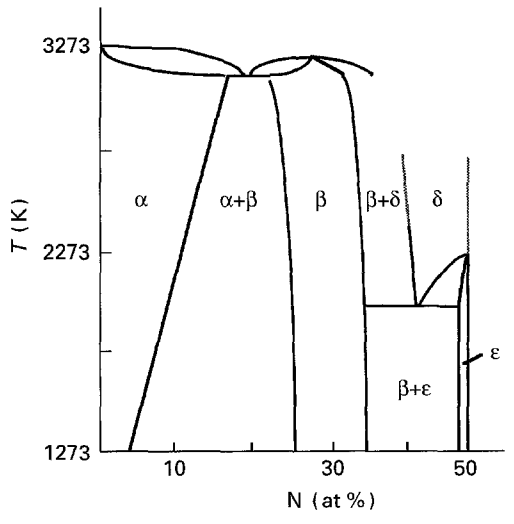

Figure 3 Tantalum–nitrogen phase diagram (after Gatterer *et al.* [4]). This work focused on the following regions: α, (α + β) and β.

The radial distribution of the volume fraction of phases present in the wire was determined in the following manner. The powder X-ray diffraction spectra of the partially nitrided tantalum (prepared from wire that had been crushed following nitridation) are shown in Fig. 5. The current application times for these three samples were 13, 102 and 500 s, respectively. In addition, a current of 20 A and a nitrogen overpressure of 0.1 MPa were used. In spectrum (a) of Fig. 5, corresponding to $t_{cur} = 13$ s, the existence of Ta_2N_{1-y} (uncircled peaks) was detected. The (1 0 1) peak of Ta_2N_{1-y} and the (1 1 0) peak of TaN_x/metallic

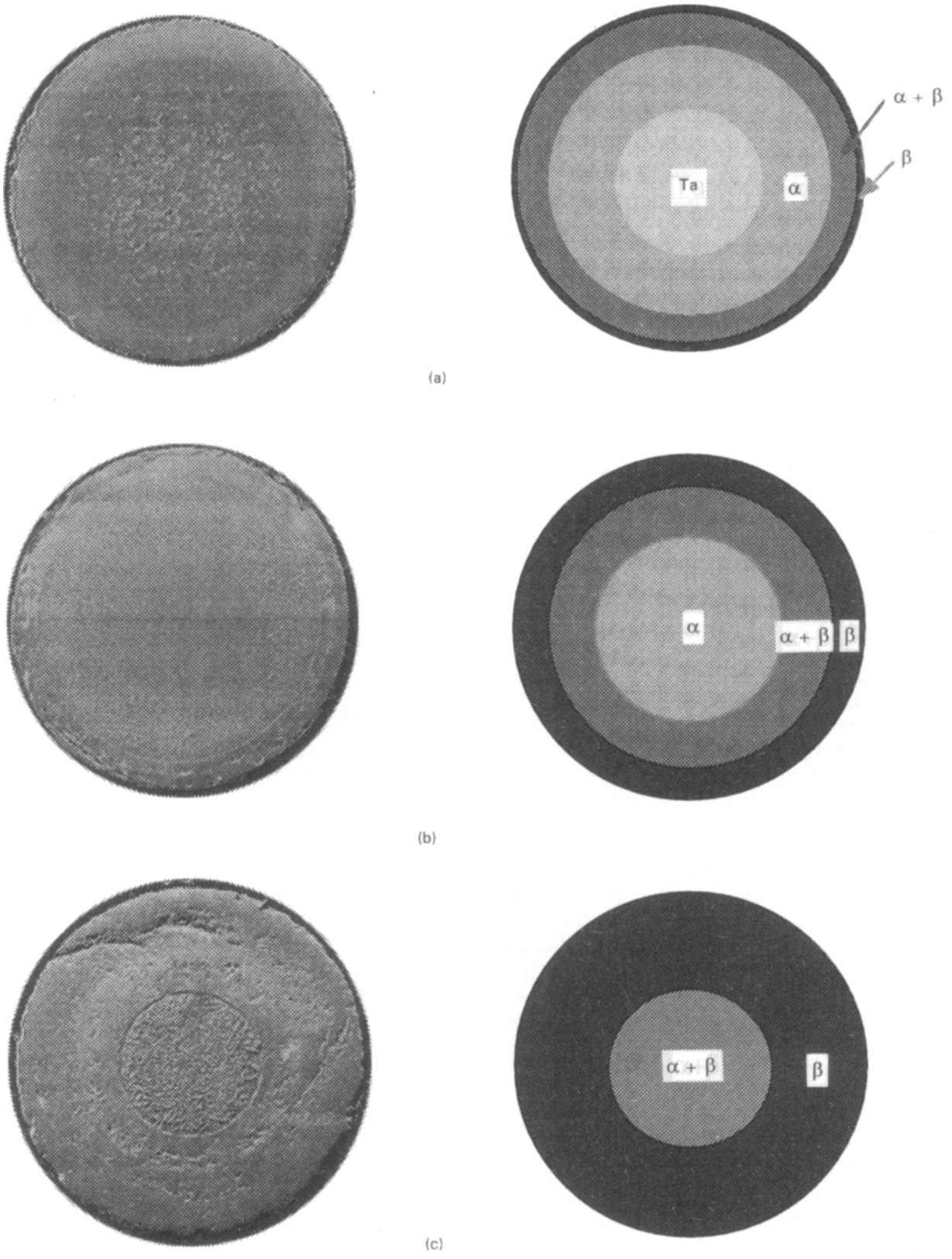

Figure 4 Scanning electron micrographs of etched cross-section of nitrided tantalum wires heated under $p_{N_2} = 0.1$ MPa and $T = 2630$ K ($i = 20$ A) for $t =$ (a) 3, (b) 17 and (c) 100 s. Also shown are the corresponding schematic representations.

tantalum were of the highest intensity and were shown to be merged in some of the spectra of the samples. For quantitative analysis of the specimen, the overlapping bands were deconvoluted using the Cauchy line shape method. The weight percentages of these two phases were estimated using the integrals under the peaks of (1 0 1) for Ta_2N_{1-y} and (1 1 0) for TaN_x. In the estimation, the reference index ratios (RIR) for Ta_2N_{1-y} and TaN_x were presumed to be the same. The amount of Ta_2N_{1-y} in that sample was estimated to be about 8 wt% and the amount of the α phase was 92 wt%. In spectrum (b) of Fig. 5, corresponding to $t_{cur} = 100$ s, the composition of the partially nitrided wire was mostly the β phase (96 wt%) while a small amount of TaN_x (4 wt%) was detected. Spectrum (c) in Fig. 5, corresponding to $t_{cur} = 500$ s, shows that the tantalum

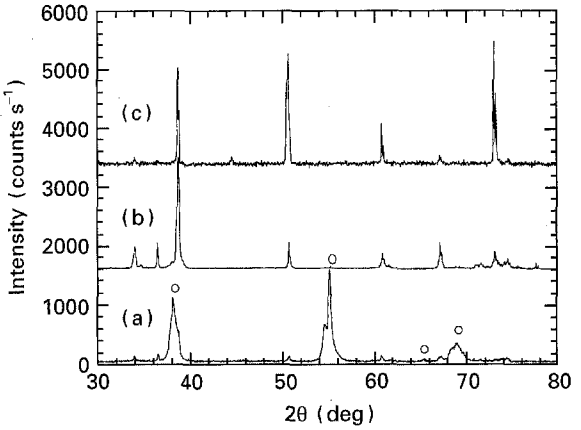

Figure 5 X-ray diffraction spectra of nitrided tantalum powder for reaction times of (a) 13 s, (b) 100 s and (c) 500 s. The peaks denoted by circles represent tantalum nitrogen solid solution, TaN_x, while the unmarked peaks are those for Ta_2Na_{1-y}.

wire sample had been fully nitrided. The time scale of 500 s is, of course, long in terms of an SHS process, but it was used here to establish the thermodynamic endpoint of the process.

3.2. Product layer growth

The dependence of the growth or disappearance of specific phases on reaction time, sample temperature, and nitrogen overpressure is listed in Table I. The phases of the samples prepared under the conditions of 20 A (corresponding to 2100 K) and 0.1 MPa nitrogen overpressure have been discussed in the previous section. At a lower temperature, $T = 1600$ K, formation of Ta_2N_{1-y} was shown to be sluggish. Although the amount of Ta_2N_{1-y} increased with time, the tantalum wire was not fully converted to Ta_2N_{1-y} at 500 s (with $p_{N_2} = 0.1$ MPa). The sample was estimated to consist of 88 wt% Ta_2N_{1-y} and 12 wt% TaN_x. At a higher temperature, $T = 2600$ K, on the other hand, the amount of Ta_2N_{1-y} increased with time initially. However, after 10 s, Ta_2N_{1-y} had apparently decomposed partially, and $Ta_4N_{1\pm z}$ had formed under the nitrogen pressure of 0.1 MPa. This suggested that $Ta_4N_{1\pm z}$ may be a stable phase with respect to Ta_2N_{1-y} at relatively high temperature (≈ 2600 K). Under higher nitrogen pressure, such as 0.5 and 0.8 MPa, the amount of Ta_2N_{1-y} increased monotonically with time at a reaction temperature of 2100 K. The tantalum wire was fully converted to Ta_2N_{1-y} after 500 s, and no TaN_x was detected in the X-ray diffraction spectra of the samples.

The growth of the β-phase layer at the surface of the partially nitrided tantalum wire may be seen in Fig. 6, which is a plot of the layer thickness following various current application times. Three sample temperatures and one nitrogen overpressure value were used. The thickness of the surface layer – measured radially inward from the surface – was determined from scanning electron micrographs of the samples following nitridation. The nitridation was considered to be complete as the product layer thickness was equal to the wire's radius. Several observations have been made. First, the effect of sample temperature on the growth rate of the surface layer was significant, particularly as the temperature was raised from 1600 K to 2100 K. The effect was less pronounced as the temperature was further increased to 2600 K. Second, a linear increase of layer thickness with time was observed. Third, the time required for complete nitridation was relatively short at the higher temperatures. Finally, the slope of each line was observed to increase as the nitrogen overpressure was increased.

TABLE I Ta_2N phase weight percentage of nitrided tantalum under various conditions

Pressure (MPa)	Current (A)	Ta_2N phase (wt %)		
		10 s	100 s	500 s
0.1	16	–	38	88
0.1	20	8	94	100
0.1	24	56	71[a]	59[a]
0.5	20	46	96	100
0.8	20	49	100	100

[a]The other phase is $Ta_4N_{1\pm z}$.

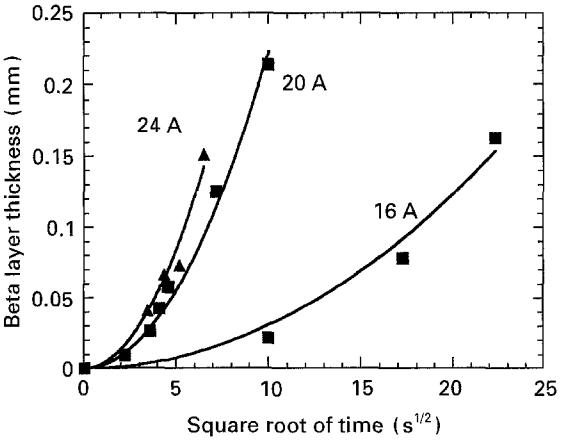

Figure 6 Tantalum nitride (Ta_2N_{1-y}) layer thickness on the surface of the reacted tantalum wire as a function of reaction time. $p_{N_2} = 0.1$ MPa.

3.3. Intrinsic reaction mechanism

Non-catalytic gas–solid reactions typically proceed by one of three mechanisms. The three mechanisms can be identified (and quantified through modelling) according to the relative magnitude of the rates of diffusional mass transfer and chemical reaction. The three mechanisms are often described by a heterogeneous (shrinking core) model, a homogeneous (spatially uniform) model, and a more general (intermediate) model, respectively [8]. In this section, each of these three models are evaluated for its applicability as the mechanism for the high-heating-rate nitridation of tantalum. Knowledge of the specific mechanism can then be used to develop a complete understanding of the SHS process.

First, the heterogeneous model was evaluated as a possible reaction mechanism. The heterogeneous (or "shrinking core") model describes a situation where two distinct layers with distinctly different material

properties are present during at least a portion of the process. The outer layer (or "skin") consists only of the reaction product, while the core consists only of the solid reactant. The chemical reaction is confined to the skin–core interface. This process is often termed a diffusion-limited process, because the flux of the reactive gas through the sample's surface is determined by the rate of diffusion to the reaction surface. Corrosion processes often occur by this mechanism. The high-heating-rate process studied in this work cannot, however, be appropriately described as a shrinking core process, because a distinct interface between the α and β phases was not observed, and a third (two-phase) region was observed. In addition, a highly simplified version of the heterogeneous model would suggest that the so-called "parabolic kinetics" should apply: a straight-line relationship between layer thickness and the square root of time should thus be observed. However, Fig. 6 clearly indicates that such a linear relationship of layer thickness versus square root of time does not exist under these conditions. Therefore, the parabolic kinetics does not apply. These two experimental observations are sufficient to eliminate the shrinking core model from further consideration.

Second, the homogeneous model was evaluated as a possible reaction mechanism. In this case, the composition inside the sample is uniform at all times during the experiment, such that the composition is independent of position. Unlike the heterogeneous model, distinct layers of skin and core, as well as a sharp and well-defined reaction surface, do not exist. This process is often termed a reaction-limited (or kinetic-limited) process, because the flux of the reactive gas through the sample's surface is determined by the volumetric rate of chemical reaction between the reactive gas and the solid reactant. Grigoriev *et al.* [7] invoked this mechanism to describe the results of a similar experiment that involved a rapidly, resistively heated metal wire in the presence of a reactive gas. This is certainly not the correct mechanism for the present case, however, because a distinct skin layer was observed throughout the process. In other words, the sample was distinctly inhomogeneous in all cases. The difference between these results and those of Grigoriev *et al.* can undoubtedly be traced to the difficulty in the latter case of obtaining detailed mechanistic information from experiments where a very fine wire ($\sim$ 100 μm diameter) was nitrided on subsecond time scales.

Third, a more general model was evaluated as a possible reaction mechanism. The general model has features of both the heterogeneous and homogeneous models. In this case, the process is neither diffusion- nor reaction-limited. The flux of the reactive gas through the sample's surface is determined by a combination of the rates of diffusion and chemical reaction (which are of similar magnitude). A skin layer may form during the process, and it may act as a fairly significant barrier to diffusion. The locus of the chemical reaction is not necessarily confined to an infinitesimally thin reaction surface, however, thereby allowing a portion of the diffusing reactive gas to diffuse radially inward, into the core. The concentration of dissolved reactive gas in the core is thus finite, and a radial gradient in the concentration of the dissolved reactive gas may or may not exist. This is, of course, similar to the generalized moving boundary problem described by Crank [9] and others [10], in which only a portion of a diffusing species adds to a growing interface and the remainder passes through the interface. Again, this is not the appropriate mechanism for the high-heating-rate gas–solid reaction experiments described above, because the appearance of a two-phase region between the single-phase skin and core regions would not be expected.

The appropriate expression for the chemical reaction mechanism must, therefore, account for the presence of the following sequence of microstructures present during the process: α-core only ($t = 0$), β-skin/two-phase ring/α-core, β-skin/two-phase core, β-skin only ($t \rightarrow \infty$). For this purpose, a so-called "twin core" model was developed to account for the presence of the two-phase ring that cannot be accounted for by the other models that were discussed in the previous paragraphs. A brief description of the physicochemical basis of the model is given here; a detailed description is given in the Appendix. The theoretical model consists of an energy and two mass continuity equations that yield time-dependent temperature, nitrogen concentration, and β-phase volume fraction profiles, respectively, when solved with appropriate initial and boundary conditions. The energy continuity equation accounts for internal conduction, ohmic heat generation, and surface losses by radiation and natural convection. The first mass balance accounts for diffusion and reaction (loss), while the second mass balance accounts for reaction (gain). The reaction is assumed to be heterogeneous, occurring only at an α/β interface. The magnitude and duration of the applied current, as well as effective transport parameters, are explicitly accounted for.

The results of calculations based on the theoretical are shown in Figs 7 and 8. Fig. 7 shows a typical radial distribution of the volume fraction of product (β) phase at various times. Again, at early times, the distribution conforms precisely to that of the moving boundary description, and deviates significantly from this description at later times. Fig. 8 shows the

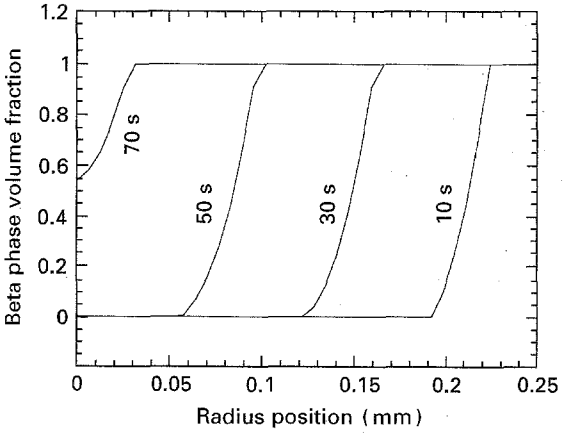

Figure 7 Typical radial distribution of the volume fraction of product, β, phase at various times.

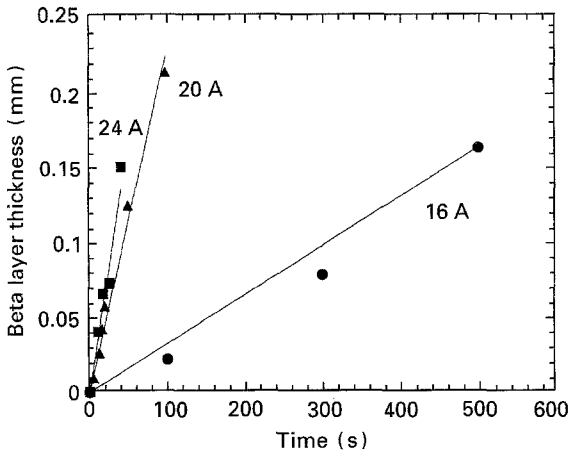

Figure 8 Position of the skin–core boundary as a function of time at 0.1 MPa N_2.

position of the skin–core boundary as a function of time. Fig. 8 highlights the fairly good agreement that was achieved between the theoretical model calculation results and the experimentally determined values.

It is, therefore, possible to deduce a detailed mechanism of the Ta–N reaction under high-heating-rate conditions. At the beginning of the process, low and intermediate temperatures are briefly present, and the diffusion and reaction processes are slow. As the temperature is further increased, diffusion in both the single-phase skin and core regions proceed at similar rates, while the reaction at the skin–core interface proceeds at a finite rate. In our case, surface nitrogen concentration is about 33 at % (β phase). When the wire is held at the maximum temperature for an intermediate time period (i.e. before complete nitridation), the core material adjacent to and radially inward from the skin–core interface (at $r = r_B^-$) may be nearly saturated with dissolved nitrogen (r is the radial position in the wire). At this point in time, the concentration at this position is, of course, too low to form the β-phase; the local composition thus remains the α-phase. The rapid cooling that follows cessation of current, however, usually results in a supersaturation of dissolved nitrogen at this point in the core near the interface. A sudden cooling of >1000 K can be expected in the first second following current cessation. This creates a strong driving force for the formation of β-phase material from nitrogen-saturated Ta–N solid solution. In addition to the macroscopic skin–core interface, seeds of the β phase must be created to relieve the supersaturation. The seeds continue to grow until a state of local saturation is achieved. The region remains a two-phase region of α and β phases (and not single-phase β), however, because the amount of nitrogen in the r_B^- region at the point of current cessation was not sufficient to completely nitride the core material during cooling. The single-phase skin and core regions, alternatively, are formed in the more usual manner.

3.4. Implications for SHS

Ultimately, the results of these high-heating-rate diffusion couple experiments are most directly useful in developing a detailed understanding of the SHS process. For example, the Ta–N_2 reaction is a non-catalytic gas–solid reaction, and may thus proceed as a simple corrosion process. This study has shown that even in the presence of a surface layer, very high nitridation rates can be achieved. The high nitridation rates lead to high rates of formation of Ta–N solid solution and the β phase. This is very important because the formation of solid solution and the β phase are significantly exothermic processes. A rapid nitridation process, therefore, gives rise to a corresponding rapid rate of heat generation, which, in turn, drives the self-propagating reaction. On the other hand, a lower local heating rate of reactants in an SHS sample leads to the formation of a skin layer that does act as a diffusion barrier. This may lead to process conditions that are not favourable to self-propagation.

These results are also directly applicable to a parallel effort in the development of a complete theoretical model of the SHS process [11]. More specifically, the reaction mechanism and corresponding reaction rate expressions are required for the development of the model. This is the portion of the SHS process that is the least well known, because the rapid heating rates and short reaction times make the quantification of the reaction kinetics an experimental impossibility in powder-based systems. The ongoing theoretical study will incorporate the results of this study in order to (i) provide a micromechanistic framework for the interpretation of experimental results, and (ii) develop a fundamental understanding of the SHS process with respect to the processing-microstructure-property relationship.

4. Conclusion

A series of very high-heating-rate diffusion couple experiments were conducted, in order to develop a detailed and quantitative understanding of the intrinsic chemical reaction kinetics of a typical gas–solid SHS reaction. A metal (tantalum) wire was heated quickly ($> 1000\,K\,s^{-1}$) by resistive heating in a reactive gas (nitrogen), thus nitriding the wire. Microstructural analysis of the wire's cross-section yielded detailed information about the extent of reaction at various times. A two-phase α + β mixture phase region was observed in nitrided samples. β-phase formation was found to occur before nitrogen-saturated α-phase formation throughout the sample. These results were compared with three existing models for non-catalytic gas–solid reaction processes. Each was shown to be inappropriate for describing these reactions that had been conducted under very high-heating-rate conditions. A theoretical model was thus developed to account for all experimental observations. Subsequent analysis showed that although the skin layer of product material forms under these conditions, it does not necessarily act as a diffusion barrier that ultimately makes the SHS process a physical impossibility.

Acknowledgements

We thank Dr R. Kudesia for conducting preliminary work on this project. This work was supported in part

by the US Army Research Office, under Grant no. DAAL03-91-G-0236, and in part by the National Science Foundation under Grant no. CTS-9114253.

Appendix: the theoretical model

A.1. Physical description of the process

A circular tantalum wire of diameter d_w is placed in a nitrogen environment that is maintained at total pressure, P. The wire is placed between electrodes, and a current, i, is passed through the wire for a specified time, t_{cur}. The wire is thus resistively heated from its initial temperature to a specified maximum temperature. The wire is held at the maximum temperature while the current is maintained. For $t > t_{cur}$, the current is no longer applied, and the temperature of the wire subsequently decreases.

When the wire's temperature is substantially above the ambient temperature, the wire absorbs nitrogen by a solution–diffusion–reaction mechanism. This process is strongly affected by temperature – which, of course, changes significantly during the course of the absorption process. More specifically, very little nitrogen would be expected to be absorbed during the initial stages of heating, as well as during the later stages of cooling. At or near the maximum temperature, however, high absorption rates would be expected. Further, the relative importance of the sub-processes (i.e. solution, diffusion and reaction) is expected to shift as the temperature is rapidly raised, held, and rapidly lowered. Finally, following cessation of the applied current, the process is rapidly quenched. This quenching effectively halts each of the sub-processes, and essentially locks in the distribution of phases, as well as the species concentration in each phase.

A properly devised theoretical model must account for each of these sub-processes, and it must properly and quantitatively describe the relative contributions of each sub-process at all times during the heating, dwell and cooling portions of the experiment.

A.2. Theoretical model

The model consists of three continuity equations [12] for conservation of energy, dissolved nitrogen and Ta_2N. The energy balance in cylindrical coordinates is

$$\rho C_P \frac{\partial T}{\partial t} = k\left[\frac{1}{r}\frac{\partial}{\partial r}\left(r\frac{\partial T}{\partial r}\right)\right] + I^2 R_e \qquad \text{(A1)}$$

where ρ, C_p and k are the local density, heat capacity and thermal conductivity of the solid, respectively, T is the local temperature, t is the time, r is the radial position in the wire, I is the current density in the wire, and R_e is the electrical resistivity. Equation A1 is subject to the following initial and boundary conditions

$$t = 0, \quad 0 \leqslant r \leqslant R_w, \quad T = T_0 \qquad \text{(A2)}$$

$$t > 0, \quad r = 0, \quad \frac{\partial T}{\partial r} = 0 \qquad \text{(A3)}$$

$$t > 0, \quad r = R_w,$$

$$-k\frac{\partial T}{\partial r} = \sigma\varepsilon(T^4 - T_\infty^4) + h_e(T - T_\infty) \qquad \text{(A4)}$$

where R_w is the radius of the wire, T_0 is the initial temperature of the wire, σ is the Boltzmann constant, ε is the total emissivity of the solid, and h_e is the natural convection heat-transfer coefficient.

The mass continuity equation for nitrogen dissolved in tantalum (as solid solution) is

$$\frac{\partial(\phi_\alpha \rho_{N\alpha})}{\partial t} = -R_{\alpha\beta}a_{\alpha\beta} + \frac{1}{r}\frac{\partial}{\partial r}\left[r\rho_\alpha\phi_\alpha D^E\frac{\partial}{\partial r}\left(\frac{\rho_{N\alpha}}{\rho_\alpha}\right)\right] \qquad \text{(A5)}$$

where ϕ_α is the local volume fraction of the α phase (that is the Ta–N solid solution : see also Fig. 8), $\rho_{N\alpha}$ is the local mass density of nitrogen in the α phase, $R_{\alpha\beta}$ is the local mass absorption rate of nitrogen from the α phase to form β-phase material, $a_{\alpha\beta}$ is the local α–β intermaterial area density, ρ_α is the intrinsic mass density of the α phase, and D^E is the effective diffusion coefficient of nitrogen in the sample (and appropriate combination of the bulk diffusivities of nitrogen in the α and β phases). Upon rearrangement, Equation A5 becomes

$$\frac{\partial x_N}{\partial t} = -\frac{a_{\alpha\beta}}{\phi_\alpha\rho_\alpha}[h_m(x_N - x_{Ns})] + D^E\left[\frac{1}{r}\frac{\partial x_N}{\partial r} + \frac{\partial^2 x_N}{\partial r^2}\right] \qquad \text{(A6)}$$

where x_N is the mass fraction of nitrogen; h_m is the mass transfer coefficient for the absorption of nitrogen from α phase to form β phase [7]; x_{Ns} is the mass fraction of nitrogen in the α phase that is in equilibrium with the β phase (a function of temperature).

Equation A6 is subject to the following initial and boundary conditions

$$t = 0, \quad 0 \leqslant r \leqslant R_w, \quad x_N = x_{N_0} \qquad \text{(A7)}$$

$$t > 0, \quad r = 0, \quad \frac{\partial x_N}{\partial r} = 0 \qquad \text{(A8)}$$

$$t > 0, \quad r = R_w, \quad x_N = x_{N^*} \qquad \text{(A9)}$$

where x_{N_0} is the initial mass fraction of nitrogen in the wire, and x_{N^*} is the mass fraction of nitrogen that is in equilibrium with the ambient nitrogen gas (that is maintained at pressure P).

Further, it should be noted that the effective diffusivity, D^E, is determined by a suitable combination of the bulk diffusivities in the α and β phases (D_α and D_β), and the local volume fraction of β (ϕ_β). For $\phi_\beta = 0$, $D^E = D_0$, and for $\phi_\beta = 1$, $D^E = D_\beta$. Otherwise, for $0 < \phi_\beta < 1$, D^E is given by [13]

$$D^E = D_1 + \left[\phi_2\Big/\left(\frac{1}{D_2 - D_1} + \frac{\phi_1}{3D_1}\right)\right] \qquad (\phi_1 > \phi_2) \qquad \text{(A10)}$$

Finally, the mass continuity equation for the local volume fraction of β (ϕ_β) is

$$\frac{\partial(\phi_\beta\rho_\beta)}{\partial t} = \nu_\beta R_{\alpha\beta}a_{\alpha\beta} \qquad \text{(A11)}$$

where ρ_β is the intrinsic mass density of the β phase, and ν_β is the stoichiometric coefficient. All other quantities are defined as above. Equation A11 is subject to the condition

$$t = 0, \quad 0 \leqslant r \leqslant R_w, \quad \phi_\beta = \phi_{\beta 0} \tag{A12}$$

As in Equation A6, Equation A11 can be re-expressed as

$$\frac{\partial \phi_\beta}{\partial t} = \frac{\nu_\rho a_{\alpha\beta}}{\rho_\beta} [h_m(x_N - x_{Ns})] \tag{A13}$$

A.3. Auxiliary quantities

In order to conduct theoretical experiments of the nitridation of tantalum under SHS-like heating conditions, additional quantities are required. First, the local material (mixture) properties are found as

$$k = \phi_\alpha k_\alpha + (1 - \phi_\alpha) k_\beta \tag{A14}$$

$$\rho = \phi_\alpha \rho_\alpha + (1 - \phi_\alpha) \rho_\beta \tag{A15}$$

$$C_p = \phi_\alpha C_{p\alpha} + (1 - \phi_\alpha) C_{p\beta} \tag{A16}$$

Second, the mass transfer coefficient, h_m, is determined as [12]

$$h_m = \frac{2(\rho_\alpha x_N) D_\alpha}{d_p} \tag{A17}$$

where d_p is the diameter of the growing β-phase grain. Third, the natural convection heat-transfer coefficient, h_e, that is required in Equation A4 is determined as follows [12]

$$N_{Nu} = a(N_{Gr} N_{Pr})^m \tag{A18}$$

where the Nusselt, Grashof and Prandtl numbers, respectively, are defined here as

$$N_{Nu} = \frac{h_e(2R_w)}{k_f} \tag{A19}$$

$$N_{Gr} = \frac{(2R_w)^3 \rho_f^2 g \beta_f \Delta T}{\mu_f^2} \tag{A20}$$

$$N_{Pr} = \frac{c_{pf} \mu_f}{k_f} \tag{A21}$$

where k_f, ρ_f, m_f, c_{pf} are the thermal conductivity, density, viscosity, and heat capacity, respectively, for the fluid phase (i.e. gaseous nitrogen). The empirically determined constants, a and m, for the case of a horizontal cylinder of circular cross-section, such that $10^{-3} \leqslant (N_{Gr} N_{Pr}) \leqslant 1$ are $a = 1.09$ and $m = 0.10$. Equation A18, with Equation A19 is then solved for h_e.

The remaining quantities required for the simulation are the material property parameters. The parameter values are listed in Tables AI and AII.

A.4. Method of solution

The continuity Equations A1, A6 and A13, along with their initial and boundary conditions, were discretized in fully implicit finite difference form. Each resulting set of equations was solved simultaneously using the Thomas method for tridiagonal matrix inversion. Details of the method have been given in great detail elsewhere [14] and are not repeated here. The calculations updated the radial distribution profiles of temperature, dissolved nitrogen concentration and β-phase volume fraction. In addition, the instantaneous location of the sink–core boundary was calculated in the usual manner [9].

TABLE AI Material property parameter values for condensed phases [15, 16]

Material property	Ta (α)	TaN_x (β)	Units
k	77.4	77.4	$W m^{-1} K^{-1}$
C_p	167.4	167.4	$J kg^{-1} K^{-1}$
ρ	16600	14400	$kg m^{-3}$
ε	0.23	0.80	–
R_e	12.5×10^{-8}	110×10^{-8}	Ωm
D_0	1.23×10^{-6}	1.5×10^{-6}	$m^2 s^{-1}$
E_D	1.7×10^5	1.2×10^5	$J mol^{-1} K^{-1}$

TABLE AII Material property parameter values for the gaseous phase [17]

Material property	Value	Units
Density, ρ_f	P/RT_f	$kg m^{-3}$
Compressibility, β_f	$1/T_f$	K^{-1}
Heat capacity, C_{pf}	$970 + 0.15 T_f$	$J kg^{-1} K^{-1}$
Viscosity, μ_f	$20 \times 10^{-5} + 3.2 \times 10^{-8} (T_f - 348)$	$kg m^{-1} s^{-1}$
Thermal conductivity, k_f	$(1.77 - 0.45/\gamma)\mu_f c_{pf}$	$W m^{-1} K^{-1}$

References

1. Z. A. MUNIR, *Am. Ceram. Soc. Bull.* **67** (1988) 342.
2. S. DEEVI and Z. A. MUNIR, *J. Mater. Res.* **5** (1990) 2177.
3. Z. A. MUNIR, *High Temp. Sci.* **27** (1990) 279.
4. J. GATTERER, G. DUFEK, P. ETTMAYER and R. KIEFFER, *Monat. Chem.* **106** (1975) 1137.
5. J. VINCENS and R. DELVIGNETTE, *Phys. Status Solidi* **A33** (1976) 497.
6. G. BRAUEU, J. WEIDLEIM and J. STRAHLE, *Z. Anorg. Allgem. Chem.* **348** (1966) 298.
7. Yu. M. GRIGORIEV, S. L. KHARATYAN, Z. S. ANDRIANOVA, A. N. IVANOVA, and A. G. MERZHANOV, *Comb. Expl. Shock Waves* **13** (1977) 713.
8. G. F. FROMENT and K. B. BISCHOFF, "Chemical reactor analysis and design" (Wiley, New York 1979).
9. J. CRANK, "The mathematics of diffusion" (Clarendon, Oxford, 1956).
10. H. S. CARSLAW and J. C. JAEGER, "Conduction of heat in solids" (Clarendon, Oxford, 1959).
11. Y. ZHANG and G. C. STANGLE, *J. Mater. Sci.* **28** (1993) 2592.
12. R. B. BIRD, W. E. STEWART and E. N. LIGHTFOOT, "Transport phenomena" (Wiley, New York, 1960).
13. Z. HASHIN, *J. Appl. Mech.* **50** (1983) 481.
14. Y. ZHANG and G. C. STANGLE, *J. Mater. Res.* **9** (1993) 2605.
15. G. L. MILLER, "Tantalum and niobium" (Butterworths, London, 1959).
16. R. C. WEAST, "Handbook of chemistry and physics", 53rd Edn (The Chemical Rubber Company, Cleveland, OH, 1972).
17. R. C. REID and T. K. SHERWOOD, "The properties of gases and liquids" (McGraw-Hill, New York, 1966).

Received 8 November 1993
and accepted 9 January 1994